Case Study 16

Detection and Visualisation of Oceanic Fronts from Satellite Data, with Applications for Fisheries, Marine Megafauna and Marine Protected Areas

Peter I. Miller[1]

16.1 Background Information

The polar-orbiting AVHRR and Aqua-MODIS infrared sensors provide frequent views of a wide range of physical processes occurring at the sea surface, including: fronts, mesoscale eddies, currents and upwelling. Remote sensing of the marine environment is an established field, exploiting satellite data to study the development and distribution of oceanic processes (e.g. Haynes et al., 1993; Peckinpaugh and Holyer, 1994), and their effect on fisheries, sea mammals, ocean margin exchange and global warming (e.g. Podesta et al., 1993; Huthnance, 1995; Bost et al., 2009). Oceanic fronts are formed at the boundary between water masses of different temperature or density, and are often associated with mixing and enhanced biological production. Fronts that extend to the sea surface may be observed by satellite if the water masses differ in temperature or colour. Identifying fronts in satellite images manually is a tedious and subjective task, so several researchers have proposed image processing algorithms to do this semi-automatically (e.g. Bardey et al., 1999; Simpson, 1990), or entirely automatically (Cayula and Cornillon, 1992). Tracking thermal features through a time-sequence of images allows sea-surface currents to be estimated (Breaker et al., 1994).

Relationships have been established between fronts and fish abundance, for instance swordfish (Podesta et al., 1993), tuna and billfish (Worm et al., 2005). In addition, Worm et al. (2005) determined a global correlation of predator diversity with fronts. Priede and Miller (2009) applied front detection techniques to reveal a strong relationship between the track of a tagged basking shark and a thermal front. The shark followed the N-S front for a whole day, keeping just to the warmer side. A 10-year time-series (30,000 satellite images) was processed and aggregated

[1]Remote Sensing Group, Plymouth Marine Laboratory, Prospect Place, Plymouth PL1 3DH, UK.
Email address: pim@pml.ac.uk

to generate a front climatology of the UK continental shelf, indicating the regions where strong fronts are most frequently observed during each season (Miller and Christodoulou, in preparation). These maps were incorporated as a proxy for pelagic biodiversity in a UK government (Defra) project to guide the designation of UK marine protected areas.

16.1.1 Compositing techniques

Oceanographic applications of visible and infrared satellite data are severely restricted by cloud cover, a limitation compositing techniques attempt to overcome by combining all cloud-free data obtained from successive orbits. Assuming the weather system maintains regular movement of cloud across the region, over sufficient time a clear view of the ocean is achieved. The required time period may be a few days or more than a month depending on the cloudiness of the region. Conventional compositing methods average all cloud-free values obtained for each location, to produce a coarse distribution of temperature or chlorophyll (Vazquez et al., 1994; Feldman et al., 1989). These are of little value for analysing mesoscale features, because any dynamic aspects will be blurred in the time-averaged composite. Also, if half of a region is clear at the start of the compositing period and the other half is clear at the end, then any underlying change in temperature or chlorophyll during that time will produce an artificial front separating the two halves, which will confuse interpretation of any genuine features.

A few authors have combined the concepts of compositing and feature detection, by superimposing the locations of all fronts detected on a sequence of images to produce a single combined map. Clusters of fronts observed at different times near the same location indicate persistent oceanic features. Such techniques have been used to investigate the abundance of swordfish in relation to fronts (Podesta et al., 1993); to describe the seasonal distribution of fronts in the Baltic Sea (Kahru et al., 1995) and off the northeast US coast (Ullman and Cornillon, 1999); and to compile a visual database of manually identified mesoscale features in the Bay of Biscay (Bardey et al., 1999). It is much more effective to detect fronts on individual scenes and then composite, rather than attempt to detect fronts based on a composite SST map.

16.2 Materials and Methods

16.2.1 Study area

For this study we have selected a dynamic shelf-break region to the north of the UK, including part of Scotland and the Shetland and Faroe islands. A branch of the Gulf Stream takes warm North Atlantic water northwards through the Faroe-Shetland Channel (FSC) towards the Norwegian current. Strong tidal currents cause

cooler well-mixed water near to the coasts, which contrasts with warmer seasonally stratified water in the North Sea.

16.2.2 Source of sea-surface temperature data

AVHRR data can be obtained in Level 1b format from NOAA's Comprehensive Large Array-data Stewardship System (CLASS: www.class.noaa.gov). Best results are obtained from the full 1.1 km resolution (termed LAC or HRPT), though if this is not available for your region of interest then 4.4 km resolution (GAC) are available. An alternative source of SST data is Aqua-MODIS, available in Level 2 format from the NASA OceanColor website, oceancolor.gsfc.nasa.gov. SST data from both AVHRR and MODIS are routinely processed and mapped for various European and global regions by the NEODAAS service hosted by PML: www.neodaas.ac.uk , and there is unrestricted access to full resolution data for the UK southwest region.

16.2.3 Data processing

We process AVHRR data using our in-house Panorama system (Miller et al., 1997), but there are modules in Erdas Imagine, or the free alternative GRASS. The processing required is first to convert the raw radiance data into cloud-masked SST estimates, then to regrid these into any required map projection. An easier process is to take the processed Aqua-MODIS SST data from the OceanColor website, and to use the free SeaDAS software to reproject the data.

16.2.4 Thermal front detection

The composite front map technique introduced in this paper initially requires the fronts to be detected on each individual satellite image. The single-image edge detection (SIED) algorithm devised by Cayula and Cornillon (1992) indicates fronts where there is a significant difference between the mean temperature of neighbouring water masses: this is a robust and completely automated method for distinguishing genuine oceanic fronts from numerous other thermal gradients on SST images. SIED is a moderately complex algorithm but is well explained by Cayula and Cornillon (1992), so I will not attempt to repeat that here. The technique has also been successfully applied to frontal analysis in other regions (Kahru et al., 1995; Podesta et al., 1993; Hickox et al., 2000; Ullman and Cornillon, 2001).

16.2.5 Composite front map techniques

Applying SIED to a typical satellite image reveals only fragments of fronts observed through the gaps in cloud cover. The composite front map approach combines the locations of frontal fragments derived from all clear sea patches in a sequence of satellite images, to produce a synoptic view of dynamic ocean features. The

compositing duration should be long enough to provide multiple observations of most genuine features, allowing them to be distinguished from artefacts, but not so long that features are obscured by multiple adjacent observations. This decision depends on the cloudiness of the region and frequency of satellite passes; the technique works best with multiple scenes each day. Seven-day thermal front maps have been found to be appropriate for typically cloudy European waters.

A front map covering more than one day cannot be regarded as a snapshot of the region, but rather as a time-lapse picture showing a series of locations for the same dynamic features. Unlike conventional SST composites, these dynamic features are not blurred and the full resolution can be retained for detailed analysis. The short-period composites used here are in contrast to previous work on combining fronts, which examined static rather than dynamic features using weeks or months of imagery at a time (e.g. Ullman and Cornillon, 1999).

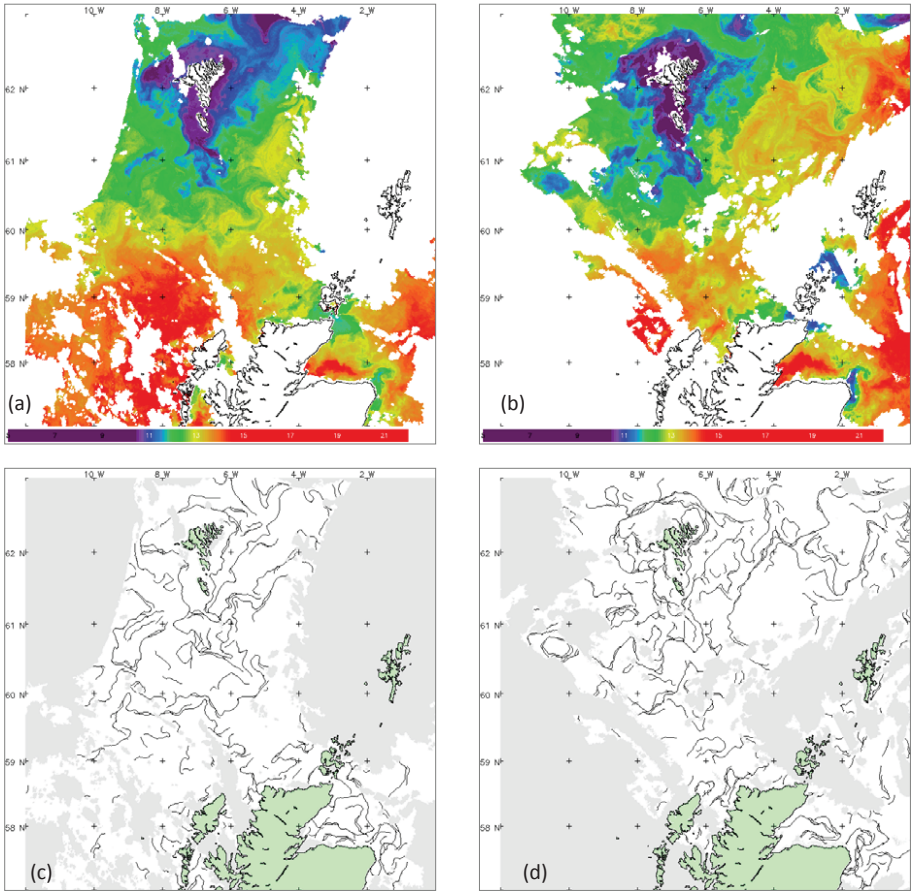

Figure 16.1 Demonstration of SIED front detection algorithm on two selected SST scenes: (a) 26 June 2009 at 06:37 GMT; (b) 27 June 2009 at 19:58 GMT; (c) Thermal fronts detected on 26 June scene, and (d) on 27 June scene.

16.2.6 Average front gradient

In order to create a composite front map it must be decided how the front segments detected on the sequence of individual images are to be combined. The simplest method would be to take the mean gradient magnitude from all fronts observed at the same pixel, ignoring any cloudy or non-front observations:

$$|\nabla(\mathrm{x},\mathrm{y},\mathrm{s})| = \begin{cases} \left[\left(\frac{\partial T(s)}{\partial x}\right)^2 + \left(\frac{\partial T(s)}{\partial y}\right)^2\right]^{1/2}, & \text{if } (\mathrm{x},\mathrm{y}) \in \mathbf{C}(s);, \quad \text{for } s \in \{1,...,S\}, (\mathrm{x},\mathrm{y}) \in \mathbf{I} \\ 0, & \text{if } (\mathrm{x},\mathrm{y}) \notin \mathbf{C}(s) \end{cases}$$

$$F_{mean}(\mathrm{x},\mathrm{y}) = \frac{\sum_{s=1}^{s} |\nabla(\mathrm{x},\mathrm{y},\mathrm{s})|}{|\{s, \text{such that } (\mathrm{x},\mathrm{y}) \in \mathbf{C}(s)\}|}, \quad \text{for } (\mathrm{x},\mathrm{y}) \in \mathbf{I}$$

$T(s)$ is one SST (or chlorophyll) map in a sequence of S scenes. $|\nabla(\mathrm{x},\mathrm{y},\mathrm{s})|$ is the gradient magnitude of the corresponding set of SIED front contour pixels $C(s)$, in degrees Kelvin per pixel distance (approx. K km^{-1}). F_{mean} is the mean composite front map derived from the sequence of S front maps. I is the set of valid image coordinates. The notation |{....}| means the number of elements in a set, so the divisor of the total magnitude is the number of scenes containing a front contour for that pixel.

16.2.7 Weighting by persistence, cloudiness and proximity

Although this simple method provides a direct estimate of the frontal gradient, it is flawed because it gives no greater weight to persistent fronts that are observed repeatedly at the same location (or slightly displaced by advection, tides or geolocation errors). The front maps therefore appear cluttered by transient or noisy segments detected on only one scene in the sequence. There are additional steps required to convert the mean temperature gradient into the full 'composite front map' metric, by weighting the gradient by the persistence, cloudiness and proximity to neighbouring features, which the reader can follow from Miller (2009). These techniques work equally well on ocean colour fields such as chlorophyll-a, on which complementary sea-surface features can be derived.

16.3 Demonstration

To facilitate this demonstration, a set of already processed and mapped AVHRR SST data for the FSC region is available on the IOCCG website at: `http://www.ioccg.org/handbook/Miller/`. The data are in PNG format, which should import easily into most GIS packages and programming languages. The data consists of 72 AVHRR SST scenes acquired between 21 and 27 June 2009, from which two scenes were selected: 26 June 2009 at 06:37 GMT and 27 June 2009 at 19:58 GMT (Figure 16.1). Note that both day and night time SST data may be combined for front detection, as

the location and gradient of fronts experience less diurnal variation than the SST values.

16.3.1 Front detection

SIED is available within the Marine Geospatial Ecology Tools (MGET: `code.nicholas.duke.edu/projects/mget`), an open source toolbox for marine researchers, so it can be downloaded and called from ArcGIS or programming languages including Python.

Apply the SIED algorithm to these SST scenes, and the output will be the detected front contours either as a raster image or as a set of vectors providing the coordinates and SST gradients along each contour. The results for the two SST scenes are shown in Figure 16.1c,d. Notice that many potential front contours are detected on each scene, and sometimes overlapping or clustered; this is as a result of overlaps in the kernel window as it is moved systematically across the whole image. Although some structures such as eddies are not fully delineated in a single scene, we will see later that the combined evidence from other scenes completes their boundaries.

There are two aspects to this algorithm which may need to be adjusted according to your application. The first is a pre-preprocessing step to smooth the SST data, to improve the appearance of the detected fronts. Cayula and Cornillon (1992) recommended a median filter to reduce noise while preserving edges, and a width of 9x9 pixels has been found to be effective in most applications. Secondly, the algorithm applies a lower limit on the mean difference in SST across a potential front. The original paper suggested a lower limit of ~0.5°C difference, though this can be reduced if weaker fronts are of interest and the SST data have low noise characteristics.

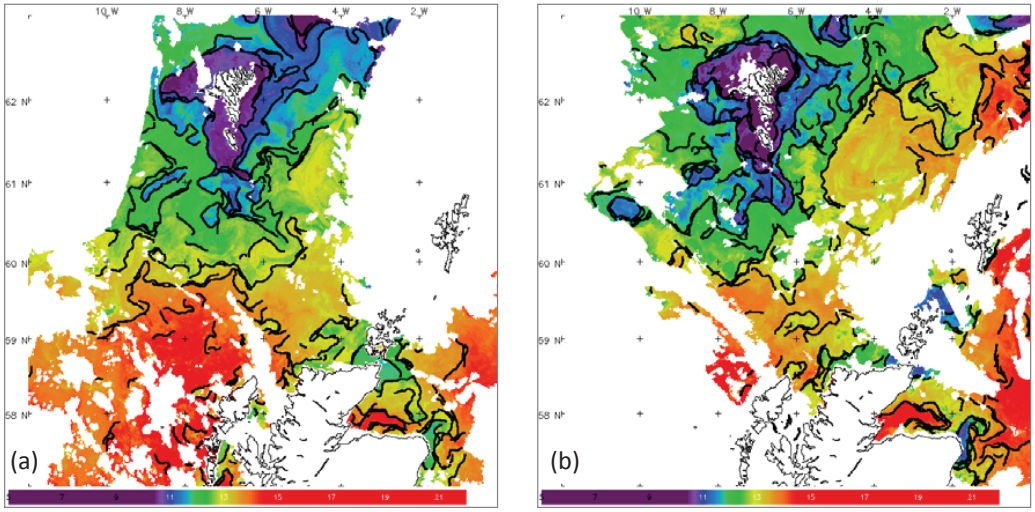

Figure 16.2 Detected thermal fronts overlaid (black lines) on SST scenes: (a) 26 June 2009 at 06:37 GMT; (b) 27 June 2009 at 19:58 GMT.

The SIED edge maps have also been overlaid as black lines onto the SST maps to demonstrate good locational accuracy of the fronts compared to the obvious SST colour gradients (Figure 16.2). It should be remembered that many genuine fronts will not be clearly seen as SST colour variations, as a single colour palette across the wide range of SST values is insufficient for revealing thermal structures that may differ by less than 1°C. If a smoothing filter is applied prior to SIED this results in slightly rounded contours.

16.3.2 Average front gradient

A single scene front map will rarely provide useful information about the physical features; most satellite passes will be a lot more cloud-covered than these examples, and also because a snapshot does not well represent the changing patterns of a dynamic system. As explained above, the next step towards a composite front map is to calculate the average front gradient over the time period, which may be as short as a few days to visualise dynamic features, or could be much longer. As in this example we are processing 98 scenes for a 7-day composite, it is clearly required to write a computer program to apply SIED to multiple SST maps.

The following code fragment (in the IDL language) assumes that you have compiled a three-dimensional array containing a stack of SIED edge maps 'gradient[x, y, z]', where each value indicates the thermal gradient if there is a front at that pixel, otherwise a missing value for cloud/land, or zero for cloud-free sea with no front. Then the average front gradient for each point (F_{mean}) is calculated:

```
FOR y = 0, height-1 DO BEGIN
   FOR x = 0, width-1 DO BEGIN
      valid_layers = WHERE (gradient[x,y,*] NE missing_val, valid_count)
      IF valid_count GT 0 THEN  $
        f_mean[x,y] = TOTAL (gradient[x,y,valid_layers]) / valid_count
   ENDFOR
ENDFOR
```

The resulting map is shown as F_{mean} in Figure 16.3, which has been coloured with a darker line colour representing a higher mean gradient (units of °C km^{-1}). At this point you can begin to appreciate the physical structures observed during that 7 days, and the varying gradient strength associated with the tidal mixing front around the coasts and weaker open ocean features.

16.3.3 Composite front map

Figure 16.3 schematically describes the remaining steps needed to combine the gradient, persistence, proximity and cloudiness information to generate a composite front map. The next stage is the persistence, P_{front}, which can be calculated easily as the ratio of fronts detected to the number of cloud-free observations, for each pixel.

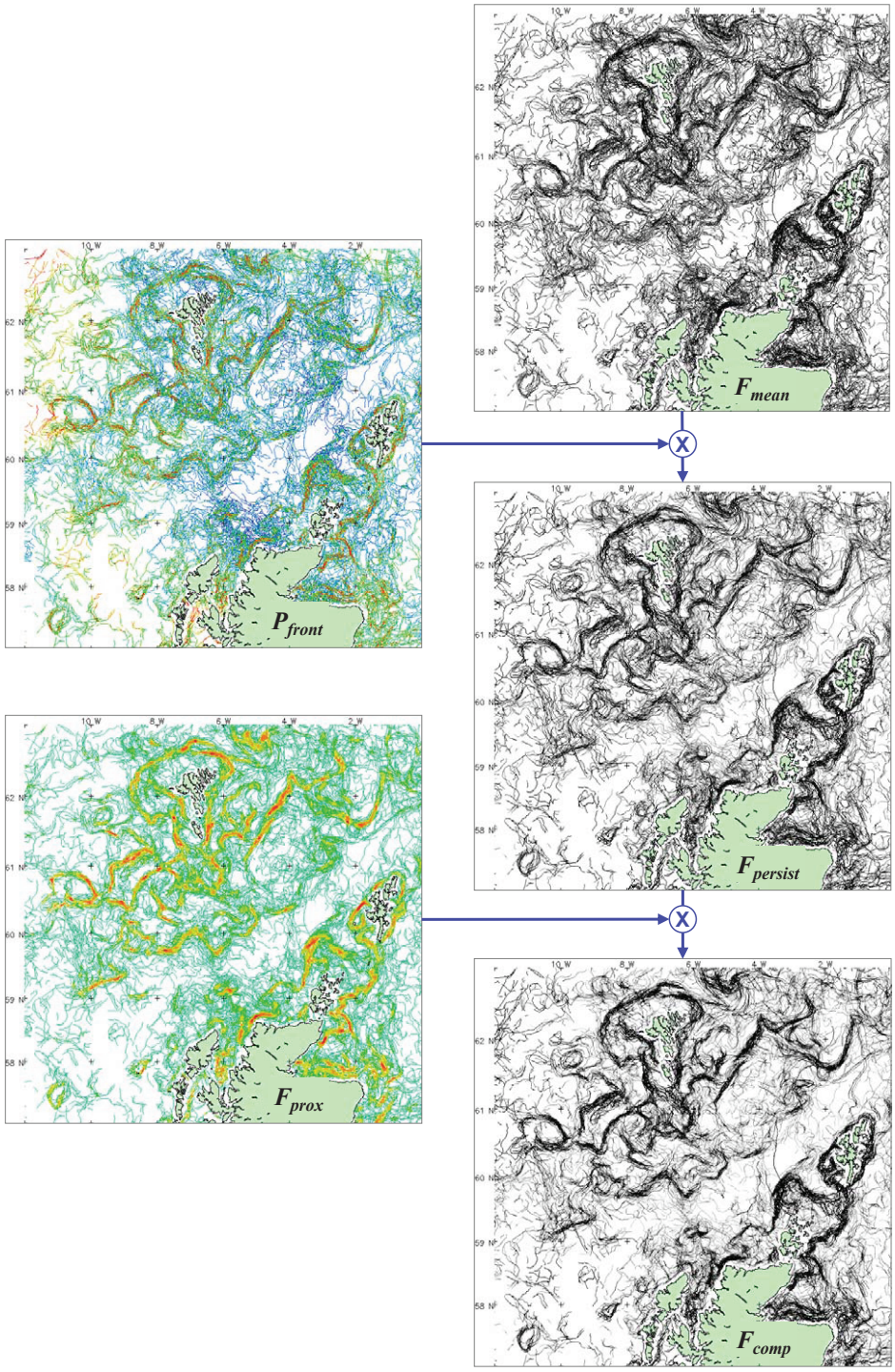

Figure 16.3 Schematic diagram of generation of composite front map for 21-27 June 2009. 98 AVHRR SST scenes within a 7-day window are processed using the SIED algorithm to detect front locations, which are then composited to calculate the mean frontal gradient F_{mean}, the probability of detecting a front P_{front}, and the evidence for a feature in proximity $Fprox$. These weighting factors are combined as the composite front map F_{comp} to provide optimal visualisation of all oceanic features observed during the period.

Hence a front which is detected a few times at a given location is rated as more significant if it was detected at every cloud-free opportunity.

Simply multiplying F_{mean} by P_{front} gives $F_{persist}$, which provides a combined measure of the gradient strength and persistence (this has no standard units). Notice how in Figure 16.3 certain features such as the shelf-break current front are clearer on the $F_{persist}$ map than in F_{mean}.

The final stage is to incorporate evidence from moving fronts, so that these are highlighted as persistent even though they affect different pixels through the time sequence. The generation of F_{prox} and F_{comp} is fully explained in (Miller, 2009) and can be implemented by a more experienced programmer. Note that the red contours in F_{prox} correspond to the clusters of fronts in the average front gradient, and that the final F_{comp} map shows the dynamic features even more clearly.

Compared to the individual SIED edge maps, the composite map depicts frontal features that are more contiguous and easier to interpret. Figure 16.4 compares the F_{comp} map against a standard SST composite for the same 7-day period; the blue ellipses indicate subtle yet important physical structures that were detected in the F_{comp} map but would have been overlooked in the SST composite. This technique is particularly powerful for revealing eddies and persistent features with weaker gradients.

A potential problem with the approach is that you get clusters of frontal lines showing multiple positions of the same feature over time. We are developing algorithms to simplify these cluttered maps (Miller, in preparation).

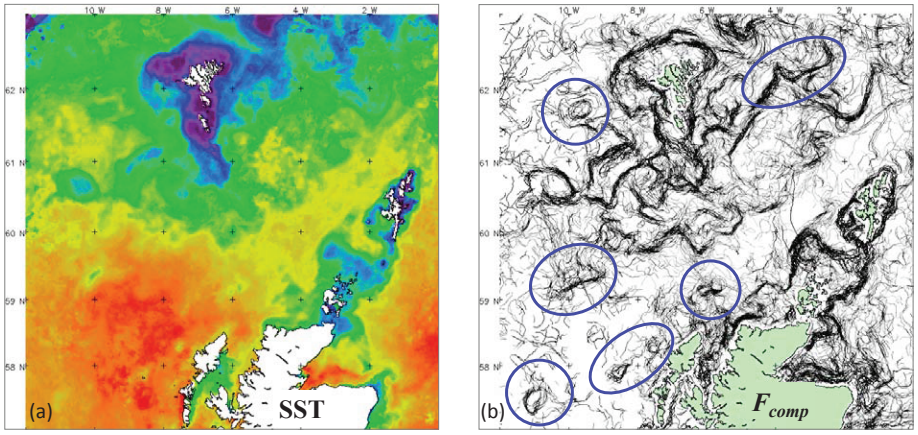

Figure 16.4 Comparison of front visualisation for 21-27 June 2009 using (a) standard SST map; and (b) composite front map. Blue ellipses indicate subtle yet important physical structures that were detected in the F_{comp} map but would have been overlooked in the SST composite.

16.4 Training and Questions

Q1. Where is the strongest thermal front detected? And is this where you would expect from viewing the SST maps?

Q2. Are there any thermal fronts shown in the SST maps that were not detected?

Q3. Are there any limitations of the SIED front detection?

Q4. What are the limitations of SST composites?

16.5 Answers

A1. The strongest fronts are observed around the Faroe, Shetland and Orkney Islands, denoting the boundary between colder tidally-mixed water and stratified warmer water. Compared to the SST map, several fronts, meanders and eddies of the shelf-break current are shown to be of similar importance in the F_{comp} map due to their persistence.

A2. On the SST map part of the shelf-break current shows a weaker front (yellow to green change) that appears more contiguous than is detected on the front map. This is probably a more diffuse mixing zone that is not defined as a front by the SIED algorithm, and the sudden colour graduations perceived in a smoothly changing colour palette can sometimes be deceptive.

A3. There is a limit on the temperature difference needed to indicate a front. The smoothing filter improves the signal-to-noise ratio of fronts, but imposes a limit on the detail of frontal contours that can be detected. Also, the smoothing makes it difficult to detect fronts close to the coast or clouds. Hence you are unlikely to detect many fronts within several kilometres of the coast, or from small patches of clear sky between clouds.

A4. As shown in Figure 16.4, a standard SST composite is not an effective tool for visualising oceanic fronts, as many dynamic or transient features may be blurred, or overlooked within a colour palette that covers a large SST range. Also the inherent variability of the background SST often causes patchy artefacts in SST composites, that may outweigh the genuine thermal structures.

16.6 References

Bardey P, Garnesson P, Moussu G, Wald L (1999) Joint analysis of temperature and ocean colour satellite images for mesoscale activities in the Gulf of Biscay. Int J Remote Sens 20(7): 1329-1341

Bost CA, Cotté C, Bailleul F, Cherel Y, Charrassin JB, Guinet C, Ainley DG, Weimerskirch H (2009) The importance of oceanographic fronts to marine birds and mammals of the southern oceans. J Mar Syst 78(3): 363-376

Breaker LC, Krasnopolsky VM, Rao DB, Yan XH (1994) The feasibility of estimating ocean surface currents on an operational basis using satellite feature tracking methods. Bull Am Meteorol Soc 75(11): 2085-2095

Cayula JF, Cornillon P (1992) Edge-detection algorithm for SST images. J Atmos Oceanic Technol 9(1): 67-80

Feldman GC, Kuring NA, Ng C et al. (1989) Ocean color: availability of the global data set. EOS 70: 634-641

Haynes R, Barton ED, Pilling I (1993) Development, persistence, and variability of upwelling filaments off the Atlantic Coast of the Iberian Peninsula. J Geophys Res - Oceans 98(C12): 22681-22692

Hickox R, Belkin I, Cornillon P, Shan Z (2000) Climatology and seasonal variability of ocean fronts in the east China, Yellow and Bohai Seas from satellite SST data. Geophys Res Lett 27(18): 2945-2948

Huthnance JM (1995) Circulation, exchange and water masses at the ocean margin: the role of physical processes at the shelf edge. Prog Oceanogr 35: 353-431

Kahru M, Hakansson B, Rud O (1995) Distributions of the sea-surface temperature fronts in the Baltic Sea as derived from satellite imagery. Cont Shelf Res 15(6): 663-679

Miller P, Groom S, McManus A, Selley J, Mironnet N (1997) Panorama: a semi-automated AVHRR and CZCS system for observation of coastal and ocean processes. RSS97: Observations and Interactions, Proc Remote Sens Soc Reading, pp 539-544

Miller PI (2009) Composite front maps for improved visibility of dynamic sea-surface features on cloudy SeaWiFS and AVHRR data. J Mar Syst 78(3): 327-336 doi:10.1016/ j.jmarsys.2008.11.019.

Miller PI (in preparation) A line clustering algorithm with application to simplifying ocean front maps derived from satellite data.

Miller PI, Christodoulou S (in preparation) Frequent locations of oceanic thermal fronts as an indicator of pelagic diversity, with application to marine protected areas.

Peckinpaugh SH, Holyer RJ (1994) Circle detection for extracting eddy size and position from satellite imagery of the ocean. IEEE Trans Geosci Remote Sens 32(2): 267-273

Podesta GP, Browder JA, Hoey JJ (1993) Exploring the association between swordfish catch rates and thermal fronts on United-States longline grounds in the Western North-Atlantic. Cont Shelf Res 13(2-3): 253-277

Priede IG, Miller PI (2009) A basking shark (*Cetorhinus maximus*) tracked by satellite together with simultaneous remote sensing II: New analysis reveals orientation to a thermal front. Fish Res 95(2-3): 370-372

Simpson JJ (1990) On the accurate detection and enhancement of oceanic features observed in satellite data. Remote Sens Environ 33(1): 17-33

Ullman DS Cornillon PC (1999) Satellite-derived sea surface temperature fronts on the continental shelf off the northeast US coast. J Geophys Res Oceans 104(C10): 23459-23478

Ullman DS, Cornillon PC (2001) Continental shelf surface thermal fronts in winter off the northeast US coast. Cont Shelf Res 21(11-12): 1139-1156

Vazquez J, Hamilton M, Van Tran A, Sumagausay R (1994) JPL Physical Oceanography DAAC reprocesses ten years of sea-surface temperature measurements from NOAA AVHRR. ESA 6: 16-17

Worm B, Sandow M, Oschlies A, Lotze HK, Myers RA (2005) Global patterns of predator diversity in the open oceans. Science 309(5739): 1365-1369